

BREAKDOWN OF KENNICUTT-SCHMIDT LAW AT GMC SCALES IN M33

SACHIKO ONODERA^{1,2}, NARIO KUNO^{1,3}, TOMOKA TOSAKI^{1,4}, KOTARO KOHNO², KOUICHIRO NAKANISHI^{3,5},
TSUYOSHI SAWADA⁵, KAZUYUKI MURAOKA⁶, SHINYA KOMUGI⁷, RIE MIURA⁸, HIROYUKI KANEKO³, AKIHIKO HIROTA¹,
AND
RYOHEI KAWABE¹

Draft version October 29, 2018

ABSTRACT

We have mapped the northern area ($30' \times 20'$) of a local group spiral galaxy M33 in $^{12}\text{CO}(J=1-0)$ line with the 45-m telescope at the Nobeyama Radio Observatory. Along with H α and Spitzer 24- μm data, we have investigated the relationship between the surface density of molecular gas mass and that of star formation rate (SFR) in an external galaxy (Kennicutt-Schmidt law) with the highest spatial resolution (~ 80 pc) to date, which is comparable to scales of giant molecular clouds (GMCs). At positions where CO is significantly detected, the SFR surface density exhibits a wide range of over four orders of magnitude, from $\Sigma_{\text{SFR}} \lesssim 10^{-10}$ to $\sim 10^{-6} M_{\odot} \text{ yr}^{-1} \text{ pc}^{-2}$, whereas the Σ_{H_2} values are mostly within $10\text{--}40 M_{\odot} \text{ pc}^{-2}$. The surface density of gas and that of SFR correlate well at a ~ 1 -kpc resolution, but the correlation becomes looser with higher resolution and breaks down at GMC scales. The scatter of the $\Sigma_{\text{SFR}}\text{--}\Sigma_{\text{H}_2}$ relationship in the ~ 80 -pc resolution results from the variety of star forming activity among GMCs, which is attributed to the various evolutionary stages of GMCs and to the drift of young clusters from their parent GMCs. This result shows that the Kennicutt-Schmidt law is valid only in scales larger than that of GMCs, when we average the spatial offset between GMCs and star forming regions, and their various evolutionary stages.

1. INTRODUCTION

Understanding the formation process of massive stars in galaxies is one of the key issues in modern astronomy because massive stars play essential roles in the evolution of galaxies. Because stars are formed from molecular gas, the study of molecular gas in galaxies provides us with important clues to the fundamental physical processes of massive star formation in galaxies. Observational studies of galaxies on global scales have shown that the surface density of star formation rate (SFR) and that of cold gas obey a simple relation, $\Sigma_{\text{SFR}} \propto \Sigma_{\text{gas}}^n$, where Σ_{SFR} is the SFR per unit area and Σ_{gas} is the surface density of gas. This relationship is known as the Kennicutt-Schmidt law (hereafter, K-S law; Schmidt 1959; Kennicutt 1998). It has been shown that the disk-averaged surface density of SFR is much better correlated with that of molecular gas Σ_{H_2} than with that of total (HI + H₂) gas $\Sigma_{\text{HI+H}_2}$ (e.g., Wong & Blitz 2002).

Because almost all of the existing studies on the K-S law have been carried out based on CO observations of kpc-scale resolution or disk-averaged data (e.g., Komugi et al. 2005), not much is known about the validity of the K-S law for smaller molecular structures such as giant molecular associations (GMAs) and giant molecular clouds (GMCs). Recently, Kennicutt et al. (2007) investigated K-S law in M51 down to a linear scale of 500 pc and cloud mass scales of $10^6\text{--}10^7 M_{\odot}$. They found that the nonlinear K-S law can be extended down to that scale. Bigiel et al. (2008) revealed that the K-S law is applicable at the 750-pc scale for seven spiral galaxies, and that it holds down to the 250-pc scale in M51. Verley et al. (2010) have shown that a loose correlation exists even in the 180-pc scale in M33, where a strong correlation was found on the global scale (Heyer et al. 2004). Because most of the molecular gas is confined within molecular clouds and virtually all of the GMCs are sites of star formation in the Milky Way, GMCs play an important role in star formation. It is important to understand how star formation at GMC scales is linked to the K-S law, which is valid for kpc-scales.

One way to address this issue is to conduct a high-spatial-resolution mapping of entire molecular gas disks in the nearest galaxies. The recent improvements in the resolution, sensitivity, and observation efficiency of radio telescopes have made such observational studies feasible.

M33 is the best target for this purpose. It is one of the nearest spiral galaxies ($D = 840$ kpc; Freedman et al. 1991) in which individual GMCs can be resolved using present-day instruments. Furthermore, because its disk is moderately face-on ($i = 51^\circ$), it is easy to study the molecular gas in relation to star formation.

Because of these desirable characteristics, M33 has been the subject of many large-scale studies of GMCs. Pioneering surveys of the central 1.7-kpc region of M33

sonodera@nro.nao.ac.jp

¹ Nobeyama Radio Observatory, National Astronomical Observatory, 462-2, Nobeyama, Minamimaki, Minamisaku, Nagano 384-1305, Japan

² Institute of Astronomy, The University of Tokyo, 2-21-1 Osawa, Mitaka, Tokyo 181-0015, Japan

³ The Graduate University for Advanced Studies (Sokendai), 2-21-1 Osawa, Mitaka, Tokyo 181-8588, Japan

⁴ Joetsu University of Education, Yamayashiki-machi, Joetsu, Niigata 943-8512, Japan

⁵ ALMA Project Office, National Astronomical Observatory, 2-21-1 Osawa, Mitaka, Tokyo 181-8588, Japan

⁶ Osaka Prefecture University, 1-1 Gakuen-cho, Nakaku, Sakai, Osaka 599-8531, Japan

⁷ Japan Aerospace Exploration Agency, Institute of Space and Astronautical Science 3-1-1 Yoshinodai, Sagami-hara, Kanagawa 229-8510, Japan

⁸ Department of Astronomy, Graduate School of Science, The University of Tokyo, 7-3-1 Hongo, Bunkyo-ku, Tokyo 113-0033, Japan

were conducted with the 12-m telescope at the National Radio Astronomy Observatory (Wilson & Scoville 1989) and the Owens Valley Radio Observatory interferometer (Wilson & Scoville 1990). They revealed that the properties of GMCs (velocity width, diameter, peak brightness temperature, and mass) were very similar to those in the Milky Way Galaxy. More recently, a CO ($J=1-0$) all-disk survey was performed with the Berkeley-Illinois-Maryland Association (BIMA) (Engargiola et al. 2003), which identified 148 GMCs with masses over $1.5 \times 10^5 M_\odot$ across the star-forming disk. The BIMA survey recovered only 20% of the CO flux in M33 because of the missing short spacings of the interferometer (Heyer et al. 2004); thus, Rosolowsky et al. (2007) performed additional CO ($J=1-0$) observations with the 45-m telescope at the Nobeyama Radio Observatory (NRO), and combined them with the existing data obtained from BIMA and the 14-m telescope at the Five College Radio Astronomy Observatory (FCRAO). They obtained the CO ($J=1-0$) map in the inner $\sim 15' \times 15'$ (~ 3.7 kpc) region at a resolution of $20''$ (~ 80 pc).

However, these observations are still insufficient to understand the overall nature of the GMCs in M33 because they do not cover the entire disk, and they possess inhomogeneities due to multi-field interferometric observations. Accordingly, a homogeneous wide-area single-dish mapping with a high spatial resolution and high sensitivity is required in order to determine the molecular gas properties of the entire disk. In order to achieve this purpose, it is effective to adopt the on-the-fly (OTF) mapping technique using a single-dish telescope having a large aperture. We performed an M33 all-disk $^{12}\text{CO}(J=1-0)$ survey with the 45-m telescope, as an NRO legacy project to study the properties and evolution of GMCs and star formation within the entire galaxy. In this paper, we investigate the K-S law in the GMC scale, which is the highest resolution (~ 80 pc) to date, as an initial result of this project.

2. OBSERVATIONS AND DATA

We observed the $^{12}\text{CO}(J=1-0)$ lines toward the north in a $30' \times 20'$ (~ 7.3 kpc \times 4.9 kpc) region of M33; the observation region covered the galactic center and the three major HII regions: NGC 604, NGC 595, and IC 133. The mapping area is shown in Fig. 1.

The observations were carried out from January to April, 2008, with the 45-m telescope at NRO. The beam size of the telescope (HPBW) was $15''$ for the rest frequency of the $^{12}\text{CO}(J=1-0)$ line (115.271204 GHz). We used the 25-BEam Array Receiver System (BEARS: Sunada et al. 2000). Because BEARS is a double sideband receiver, we measured the sideband ratios of each beam of BEARS by observing a bright standard source NGC 7538 using both BEARS and a single-beam receiver S100 equipped with a single sideband filter. The errors in the scaling factors of BEARS were smaller than $\sim 20\%$. The main beam efficiency measured with S100 was $\eta_{\text{MB}} = 0.32 \pm 0.02$ at 115 GHz. The typical system temperature was ~ 700 K (SSB). We used digital autocorrelators as backends. The spectrometers have 1024 channels covering a bandwidth of 512 MHz with a frequency resolution of 1.0 MHz, which corresponds to 1332 km s $^{-1}$ and 2.6 km s $^{-1}$. The chopper-wheel technique was employed to calibrate the antenna temperature T_A^* . Here-

after, all the CO intensity measurements are mentioned in the $T_{\text{MB}} (\equiv T_A^*/\eta_{\text{MB}})$ scale.

The observations were performed using the OTF observation mode (Sawada et al. 2008). Throughout the observations, the data were sampled every 0.1 s. The emission-free ‘‘OFF’’ points were taken at an offset of $30'$ from the center. We checked the pointing accuracy every hour with a 5-point observation of a SiO maser source IRC+30021 with a 43 GHz SIS receiver (S40). We excluded all the data in the observation sequence that had pointing errors larger than $7''.5$ or wind speed $V > 10$ m s $^{-1}$ to avoid systematic intensity loss due to pointing errors. After these data screenings, the net integration time was determined to be approximately 130 h.

The data reductions were made with the OTF reduction software package NOSTAR, which was implemented by the NRO. The data were convolved with a Gaussian-tapered Jinc function to create the spectral data cube. The grid spacing was taken as $7''.5$, and the spatial resolution of the final map was $19''.3$. Finally, the baselines were fitted and subtracted from the data cube. The velocity resolution of the final cube is 2.5 km s $^{-1}$. The rms noise in a velocity channel was 130 mK. The rms noise in the integrated intensity map was 1.6 K km s $^{-1}$, which corresponds to a mass sensitivity of $4.8 M_\odot$ pc $^{-2}$.

3. RESULTS

3.1. CO ($J=1-0$) Map

Fig. 1 shows the CO ($J=1-0$) integrated intensity map of our observation field for M33. It reveals the clumpy nature of the molecular gas distribution. The size of these clumps ranges from $\lesssim 100$ pc (comparable to our beam size) to 500 pc, which corresponds to that of GMCs and/or GMAs. The northern arm that can be traced from $(\alpha, \delta) = (1^{\text{h}}33^{\text{m}}40^{\text{s}}, +30^\circ46'0'')$ to $(1^{\text{h}}34^{\text{m}}30^{\text{s}}, +30^\circ49'0'')$ is prominent.

The surface mass density of molecular hydrogen was estimated by applying the ^{12}CO -to- H_2 conversion factor, $X_{\text{CO}} = 3 \times 10^{20}$ cm $^{-2}$ (K km s $^{-1}$) $^{-1}$ (Wilson & Scoville 1990) as follows:

$$\left(\frac{\Sigma_{\text{H}_2}}{M_\odot \text{ pc}^{-2}}\right) = 4.81 \left(\frac{X_{\text{CO}}}{3 \times 10^{20} \text{ cm}^{-2} (\text{K km s}^{-1})^{-1}}\right) \times \left(\frac{I_{\text{CO}}}{\text{K km s}^{-1}}\right) \cos i, \quad (1)$$

where i is the inclination angle of the galaxy ($i = 51^\circ$).

3.2. Star Formation Rate

We calculated the SFR using the relation between the extinction-corrected $\text{H}\alpha$ line emission and the SFR, as presented in Calzetti et al. (2007):

$$\text{SFR}(M_\odot \text{ yr}^{-1}) = 5.3 \times 10^{-42} [L(\text{H}\alpha)_{\text{obs}} + (0.031 \pm 0.006)L(24 \mu\text{m})], \quad (2)$$

in turn leading to

$$\Sigma_{\text{SFR}}(M_\odot \text{ yr}^{-1} \text{ pc}^{-2}) = 5.0 \times 10^{-5} [\Sigma(\text{H}\alpha)_{\text{obs}} + (0.031 \pm 0.006)\Sigma(24 \mu\text{m})] \cos i, \quad (3)$$

where the luminosities are in erg s^{-1} and $L(24\ \mu\text{m})$ is expressed as $\nu L(\nu)$. The unit of $\Sigma(\text{H}\alpha)_{\text{obs}}$ and $\Sigma(24\ \mu\text{m})$ is $\text{erg s}^{-1}\ \text{cm}^{-2}$.

We use the $\text{H}\alpha$ image of M33 as given by Hoopes & Walterbos (2000). It was obtained using the 0.6-m Burrell-Schmidt telescope at the Kitt Peak National Observatory. The dimensions of the CCD are 2048×2048 with a pixel size of $2''.03$ and the total field of view is approximately $70' \times 70'$. The sensitivity is $0.8 \times 10^{-17}\ \text{erg s}^{-1}\ \text{cm}^{-2}\ \text{arcsec}^{-2}$ (Hoopes et al. 2001).

We retrieved the 24- μm Multiband Imaging Photometer (MIPS: Rieke et al. 2004) datasets (AORs 3647744, 3648256, 3648512, 3648768) of the basic calibrated data (BCD) created by the Spitzer Science Center (SSC) pipeline from the Spitzer Space Telescope (Werner et al. 2004) data archive. The mosaics were assembled by gathering all the BCDs except the first data frames of each observation because they have shorter integration times. The individual calibrated frames were processed using MOPEX (Makovoz & Khan 2005) for cosmic-ray rejection and background matching was applied to overlapping fields of view. The final dimension of the each mosaic was $21' \times 89'$. After we removed the zodiacal light, and the noisy pixels near the edges by trimming, the four images were aligned with their coordinates and combined. The FWHM of point spread function is $5''.7$.

The $\text{H}\alpha$ and 24- μm images were convolved into the same angular resolution as the $\text{CO}(J=1-0)$ data ($19''.3$), regridded to $7''.5$ per pixel, and trimmed to match the $\text{CO}(J=1-0)$ map. The rms noise is $5 \times 10^{-7}\ \text{erg s}^{-1}\ \text{cm}^{-2}$ in the $\text{H}\alpha$ map, and $3 \times 10^{-5}\ \text{erg s}^{-1}\ \text{cm}^{-2}$ in the 24- μm map. The resultant SFR image is shown in Fig. 2 with the overlaid $\text{CO}(J=1-0)$ contours. The rms noises in the $\text{H}\alpha$ and 24- μm maps result in a Σ_{SFR} error and a sensitivity limit of $5 \times 10^{-11}\ M_{\odot}\ \text{yr}^{-1}\ \text{pc}^{-2}$.

Fig. 2 reveals a striking variety of star formation properties. In regions where CO emission is detected, there is a large dispersion in the values of Σ_{SFR} of over four orders of magnitude. For example, the most massive GMC at $(\alpha, \delta) = (1^{\text{h}}33^{\text{m}}9^{\text{s}}.6, +30^{\circ}49'7''.3)$ has little star formation activity despite the large amount of molecular gas it contains. In the three major star-forming regions (NGC 604, NGC 595, and IC 133), there is a considerable difference in the amount of molecular gas associated with these star-forming regions. NGC 604 has its associated GMCs at the same position, NGC 595 has the ones offset from it, and moreover, none of the GMCs are associated with IC 133.

4. DISCUSSION

Fig. 3 presents the relationship between the SFR and molecular hydrogen surface densities for four angular resolutions: $19''.3$ ($\sim 80\ \text{pc}$), $60''$ ($\sim 240\ \text{pc}$), $120''$ ($\sim 500\ \text{pc}$), and $240''$ ($\sim 1\ \text{kpc}$). The panel of $\sim 80\ \text{pc}$ resolution is the K-S law plot with the highest spatial resolution for an extra-galaxy to date. Fig. 3 shows that apparent correlations exist between Σ_{H_2} and Σ_{SFR} at the $\sim 1\ \text{kpc}$ resolution, as already found in the disk-averaged data of M33 (Heyer et al. 2004). The best least-squares fit for the $\sim 1\ \text{kpc}$ resolution data with $\Sigma_{\text{H}_2} > 2\sigma$ is

$$\log \Sigma_{\text{SFR}} = (1.18 \pm 0.11) \log \Sigma_{\text{H}_2} - (9.38 \pm 0.05). \quad (4)$$

We have fitted the power law only to the data at the 1-kpc resolution, because the data at the other resolutions

have a significant selection bias due to the omission of data points having $\Sigma_{\text{H}_2} < 2\sigma$. The selection bias makes the correlation slopes appear steeper than real.

Fig. 3 also shows that the correlation becomes looser with higher resolution, and it is hardly visible in the plot for $\sim 80\ \text{pc}$ resolution. Although most Σ_{H_2} values lie within $10\text{--}40\ M_{\odot}\ \text{pc}^{-2}$ where $\Sigma_{\text{H}_2} > 2\sigma$, Σ_{SFR} values exhibit a wide range of over four orders of magnitude, from $\lesssim 10^{-10}$ to $\sim 10^{-6}\ M_{\odot}\ \text{yr}^{-1}\ \text{pc}^{-2}$, indicating that the K-S law becomes invalid at this resolution. That is, the K-S law is valid only for averaging SFR and gas mass in large scales of several hundred parsecs. Our resolution, $\sim 80\ \text{pc}$ is smaller than these scales.

We have examined the effects of stochasticity on the estimation of SFR due to small sampling at high spatial resolutions. The initial mass function is not fully populated when smaller regions that contain only a few stars in clusters are sampled. Thus, in regions with weaker extinction-corrected $\text{H}\alpha$ emission, this effect may lead to significant scatter in the estimated Σ_{SFR} . We have estimated the significance of this effect on the 80-pc resolution data. For instance, $\Sigma_{\text{SFR}} = 10^{-9}\ M_{\odot}\ \text{yr}^{-1}\ \text{pc}^{-2}$ corresponds to the total flux of extinction-corrected $\text{H}\alpha$ emission having $L(\text{H}\alpha)_{\text{corr}} = 6.6 \times 10^{35}\ \text{erg s}^{-1}$ within the 80-pc beam. Assuming a gas temperature of $10^4\ \text{K}$ and an electron density of $100\ \text{cm}^{-3}$ in HII regions, the ionizing photon flux is given by $Q(\text{H}^0) = 7.3 \times 10^{11}\ L(\text{H}\alpha)_{\text{corr}}\ \text{s}^{-1}$ (Kennicutt 1988; Brocklehurst 1971). Therefore, the corresponding total ionizing photon flux is $Q(\text{H}^0) = 4.9 \times 10^{48}\ \text{s}^{-1}$. According to Fig. 3 in Cerviño et al. (2002), $Q(\text{H}^0)$ per unit mass varies with cluster age from 10^{47} to $10^{44}\ \text{s}^{-1}\ M_{\odot}^{-1}$. The ratio of the error in $Q(\text{H}^0)$ to the mean value, $\sigma[Q(\text{H}^0)]/Q(\text{H}^0)$, is $\sim 10M^{-1/2}$ (the ratio can vary by a factor ~ 2 depending on the cluster age), where M is the cluster mass. Thus, the cluster mass required to produce the ionizing flux mentioned above is estimated to be 50 to $5 \times 10^4\ M_{\odot}$, which results in $\sigma[Q(\text{H}^0)]/Q(\text{H}^0) \approx 1$ to 0.04. In summary, in the 80-pc scale, the error due to the effect of stochasticity at $\Sigma_{\text{SFR}} = 10^{-9}\ M_{\odot}\ \text{yr}^{-1}\ \text{pc}^{-2}$ is $\approx 0.04\text{--}1 \times 10^{-9}\ M_{\odot}\ \text{yr}^{-1}\ \text{pc}^{-2}$. The error decreases with larger Σ_{SFR} and lower spatial resolutions. For example, the maximum $\sigma[Q(\text{H}^0)]/Q(\text{H}^0)$ in the 80-pc scale is 1, 0.4, and 0.1, and in the 240-pc scale it is 0.5, 0.1, and 0.05 for $\Sigma_{\text{SFR}} = 10^{-9}, 10^{-8},$ and $10^{-7}\ M_{\odot}\ \text{yr}^{-1}\ \text{pc}^{-2}$, respectively. Although the error is significant at smaller Σ_{SFR} at the 80-pc resolution, it cannot explain the scatter of over four orders of magnitude in Σ_{SFR} .

Now, we consider the possible causes for the breakdown of the K-S law at high spatial resolutions. In grand design spiral galaxies, we often see a systematic offset between the molecular gas arms and the star forming arms as a result of the density wave and the time delay between the accumulation of gas and its ionization by newborn stars (e.g., Egusa et al. 2009). If such an offset exists in M33, it may result in the breakdown of the K-S law when we observe the galaxy with a spatial resolution comparable to the offset. However, there is no such systematic offset between the CO and the star-forming arm in M33, as shown in Fig. 2. Therefore, the offset can be ruled out as a cause.

In the Milky Way, young clusters recede from their parent GMCs with velocities of at least $\sim 10\ \text{km s}^{-1}$

(Leisawitz et al. 1989). As they evolve, the separation between clusters and their parent GMCs becomes significant and is expected to be ~ 100 pc at a cluster age of ~ 10 Myr. This drift scale is comparable to our resolution, ~ 80 pc, and thus, the separation could well lead to the scatter in our plot. However, the existence of HII regions without neighboring GMCs and GMCs without neighboring HII regions in M33, such as the ones mentioned in the previous section, cannot be explained by drift alone.

The other cause is the difference in evolutionary stages. As we have shown in Fig. 2, there is a large diversity in the star formation activity among GMCs. Some GMCs in the Milky Way are at least partially consumed and dissociated by newborn clusters (Leisawitz et al. 1989). Such GMCs are shown in Fig. 2 (i.e., the GMC at $(\alpha, \delta) = (1^{\text{h}}34^{\text{m}}17^{\text{s}}, 30^{\text{d}}52^{\text{m}}00^{\text{s}})$). The diversity among GMCs arises from the evolutionary stages that each GMC goes through, as has been shown in the most active star forming region NGC 604 (Miura et al. 2010). Chen et al. (2010) studied the relation between Σ_{SFR} and $\Sigma_{\text{HI}+\text{H}_2}$ in LMC for six GMCs in different stages of evolution, which are determined from the association of the underlying stellar population. They also found a large scatter in Σ_{SFR} , which exhibits a range of two orders of magnitude whereas the $\Sigma_{\text{HI}+\text{H}_2}$ lies within a factor of two. Kawamura et al. (2009) classified molecular clouds in the LMC into three types according to the activities of massive star formation: those with no signature of massive star formation, those with relatively small HII region(s), and those with both HII region(s) and young stellar cluster(s). They concluded that there is a sequential relation between these three types. That is, molecular clouds are first formed; then, stars are formed in the molecular clouds; and finally, the newborn stars consume and dissociate the surrounding gas. This scenario is also applicable to M33, as can be shown in NGC 604 by comparing it with warm/dense gas traced by CO ($J=3-2$) lines (Tosaki et al. 2007).

Note that the extinction-corrected H α emission is not really an appropriate tracer of SFR at resolutions as high as ~ 80 pc, because there is a spatial displacement between ionizing stars and the surrounding HII gas. According to Relaño & Kennicutt (2009), the displacement is ~ 10 pc to 50 pc in M33, and there is a radial gradi-

ent of emission from the center to the boundary of HII regions; in the order of ultraviolet, H α , 24 μm , and CO emission. Because of the radial gradient, the separations between ionizing stars and CO are larger than that between H α and CO. Thus, the “real” SFR would produce an even larger scatter in the K-S law plot for the ~ 80 -pc resolution. The contribution of dust heating from older stars to the 24- μm emission can also be responsible for the scatter, although its effect is minor.

Owing to our spatial resolution, which is comparable in scale to that of GMCs, we have clearly revealed the variety in the evolutionary stages among GMCs. The different evolutionary stages of GMCs are the main cause of deviations from the K-S law. The higher the spatial resolution, the more individual star-forming regions and molecular clouds we can resolve, and the larger the deviations seen in the K-S law plots.

5. SUMMARY

We conducted on-the-fly mapping of the northern part of M33 ($30' \times 20'$) in ^{12}CO ($J=1-0$) lines with the 45-m telescope at the Nobeyama Radio Observatory (NRO). We tested the relationship between the surface density of molecular gas mass and the SFR in an external galaxy with the highest resolution (~ 80 pc) to date. We found that the star-forming activities in the GMC scale exhibit a wide range of over four orders of magnitude at positions where CO is significantly detected, such that $\Sigma_{\text{SFR}} \lesssim 10^{-10}$ to $\sim 10^{-6} M_{\odot} \text{yr}^{-1} \text{pc}^{-2}$, whereas their Σ_{H_2} values are mostly in the range of 10–40 $M_{\odot} \text{pc}^{-2}$. We also found that the K-S law of H $_2$ gas, $\Sigma_{\text{SFR}} \propto \Sigma_{\text{H}_2}^n$, becomes invalid at GMC scales (~ 80 pc). The breakdown of the K-S law is attributed to the difference in the evolutionary stages of GMCs and the drift of newborn clusters from their parent GMCs that become apparent at this spatial resolution.

We thank the referee, Robert Kennicutt, for his prompt report and for his helpful comments, which improved our work. We also thank Rene Walterbos for providing us with the H α image of M33. S. O. was financially supported by the Global COE Program “The Physical Sciences Frontier,” MEXT, Japan. The Nobeyama Radio Observatory is a branch of the National Astronomical Observatory of Japan, National Institutes of Natural Sciences.

REFERENCES

- Brocklehurst, M. 1971, *MNRAS*, 153, 471
 Bigiel, F., Leroy, A., Walter, F., Brinks, E., de Blok, W. J. G., Madore, B., & Thornley, M. D. 2008, *AJ*, 136, 2846
 Calzetti, D., et al. 2007, *ApJ*, 666, 870
 Cerviño, M., Valls-Gabaud, D., Luridiana, V., & Mas-Hesse, J. M. 2002, *A&A*, 381, 51
 Chen, C. - R., et al. 2010, arXiv:1007.5326
 Egusa, F., Kohno, K., Sofue, Y., Nakanishi, H., & Komugi, S. 2009, *ApJ*, 697, 1870
 Engargiola, G., Plambeck, R. L., Rosolowsky, E., & Blitz, L. 2003, *ApJS*, 149, 343
 Freedman, W. L., Wilson, C. D., & Madore, B. F. 1991, *ApJ*, 372, 455
 Heyer, M. H., Corbelli, E., Schneider, S. E., & Young, J. S. 2004, *ApJ*, 602, 723
 Hoopes, C. G., & Walterbos, R. A. M. 2000, *ApJ*, 541, 597
 Hoopes, C. G., Walterbos, R. A. M., & Bothun, G. D. 2001, *ApJ*, 559, 878
 Kawamura, A., et al. 2009, *ApJS*, 184, 1
 Kennicutt, R. C., Jr. 1988, *ApJ*, 334, 144
 Kennicutt, R. C., Jr. 1998, *ApJ*, 498, 541
 Kennicutt, R. C., Jr., et al. 2007, *ApJ*, 671, 333
 Komugi, S., Sofue, Y., Nakanishi, H., Onodera, S., & Egusa, F. 2005, *PASJ*, 57, 733
 Leisawitz, D., Bash, F. N., & Thaddeus, P. 1989, *ApJS*, 70, 731
 Makovoz, D., & Khan, I. 2005, in *ASP Conf. Ser.* 347, *Astronomical Data Analysis Software and Systems XIV*, ed. P. Shopbell, M. Britton, & R. Ebert, 81
 Miura, R., et al. 2010, *ApJ*, submitted.
 Relaño, M., & Kennicutt, R. C. 2009, *ApJ*, 699, 1125
 Rieke, G. H., et al. 2004, *ApJS*, 154, 25
 Rosolowsky, E., Keto, E., Matsushita, S., & Willner, S. P. 2007, *ApJ*, 661, 830

- Sawada, T., et al. 2008, PASJ, 60, 445
Schmidt, M. 1959, ApJ, 129, 243
Sunada, K., Yamaguchi, C., Nakai, N., Sorai, K., Okumura, S. K.,
& Ukita, N. 2000, in CPIE Conf. Ser. ed. H. R. Butcher, 4015,
237
Tosaki, T., Miura, R., Sawada, T., Kuno, N., Nakanishi, K.,
Kohno, K., Okumura, S. K., & Kawabe, R. 2007, ApJ, 664, L27
Verley, S., Corbelli, E., Giovanardi, C., & Hunt, L. K. 2009,
A&A, 493, 453
Verley, S., Corbelli, E., Giovanardi, C., & Hunt, L. K. 2010,
A&A, 510, A64
Werner, M. W., et al. 2004, ApJS, 154, 1
Wilson, C. D., & Scoville, N. 1989, ApJ, 347, 743
Wilson, C. D., & Scoville, N. 1990, ApJ, 363, 435
Wong, T., & Blitz, L. 2002, ApJ, 569, 157

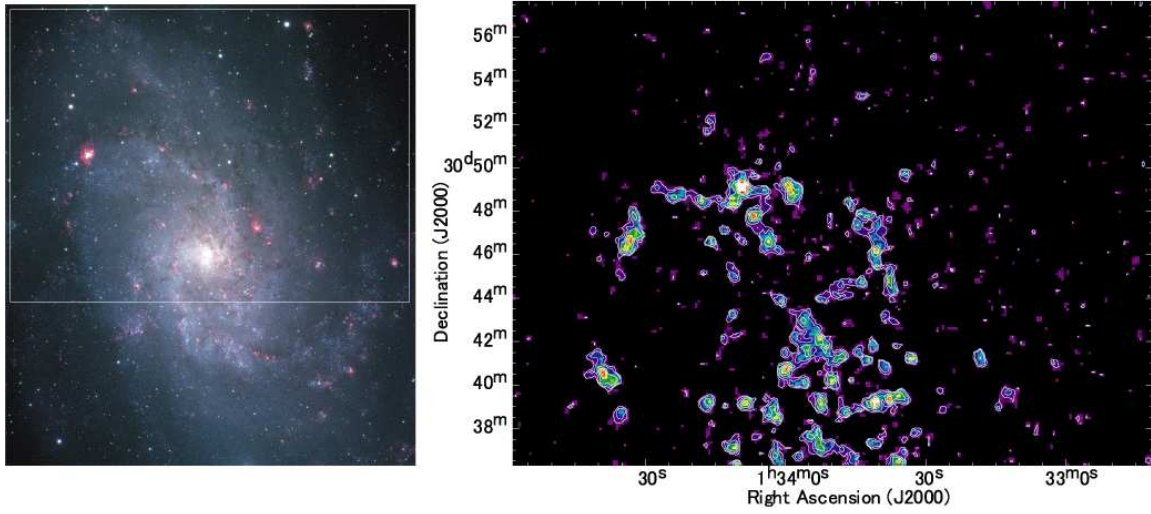


FIG. 1.— (Left) BVH α image of M33 taken with SUBARU Suprime-Cam: courtesy of V. Vasevicius, S. Okamoto, and N. Arimoto. The rectangle represents our mapping area of CO ($J=1-0$) ($30' \times 20'$). (Right) Smoothed and clipped integrated intensity map of the CO ($J=1-0$) lines. The contour levels are 1, 2, 4, 6, and 8 K km s $^{-1}$, respectively.

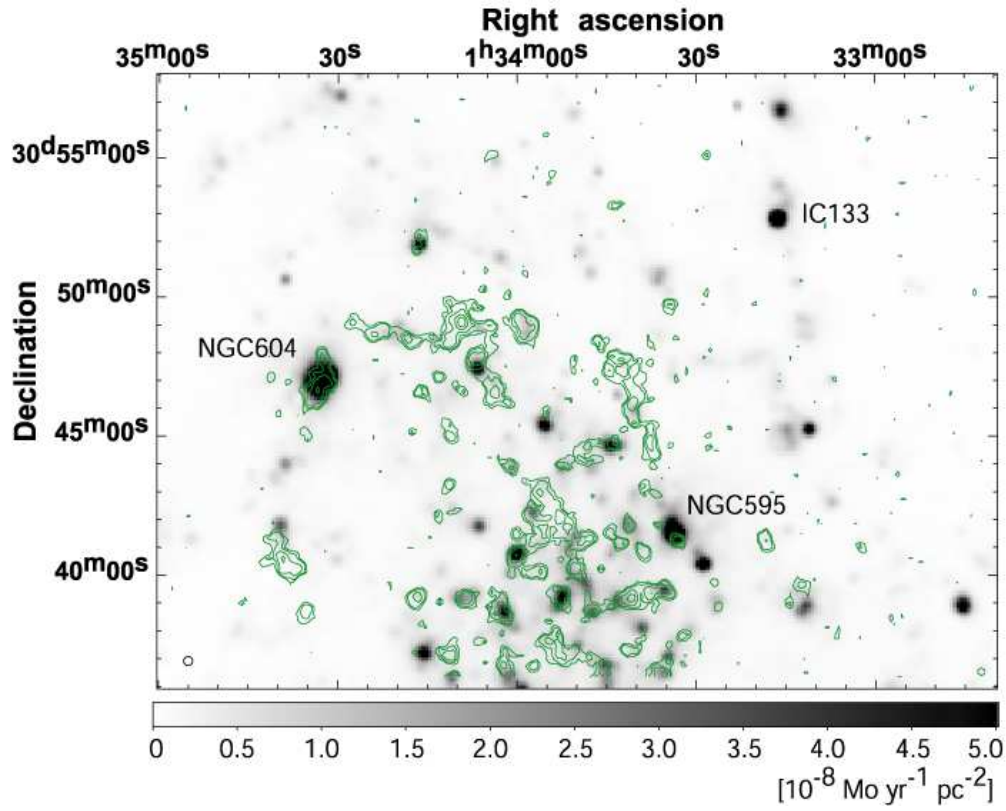


FIG. 2.— CO integrated intensity map (contour) overlaid on the SFR map convolved into $19''.3$ resolution. The contour levels are 1, 2, 4, 8, and 16 K km s $^{-1}$. The circle at bottom left represents the beam size.

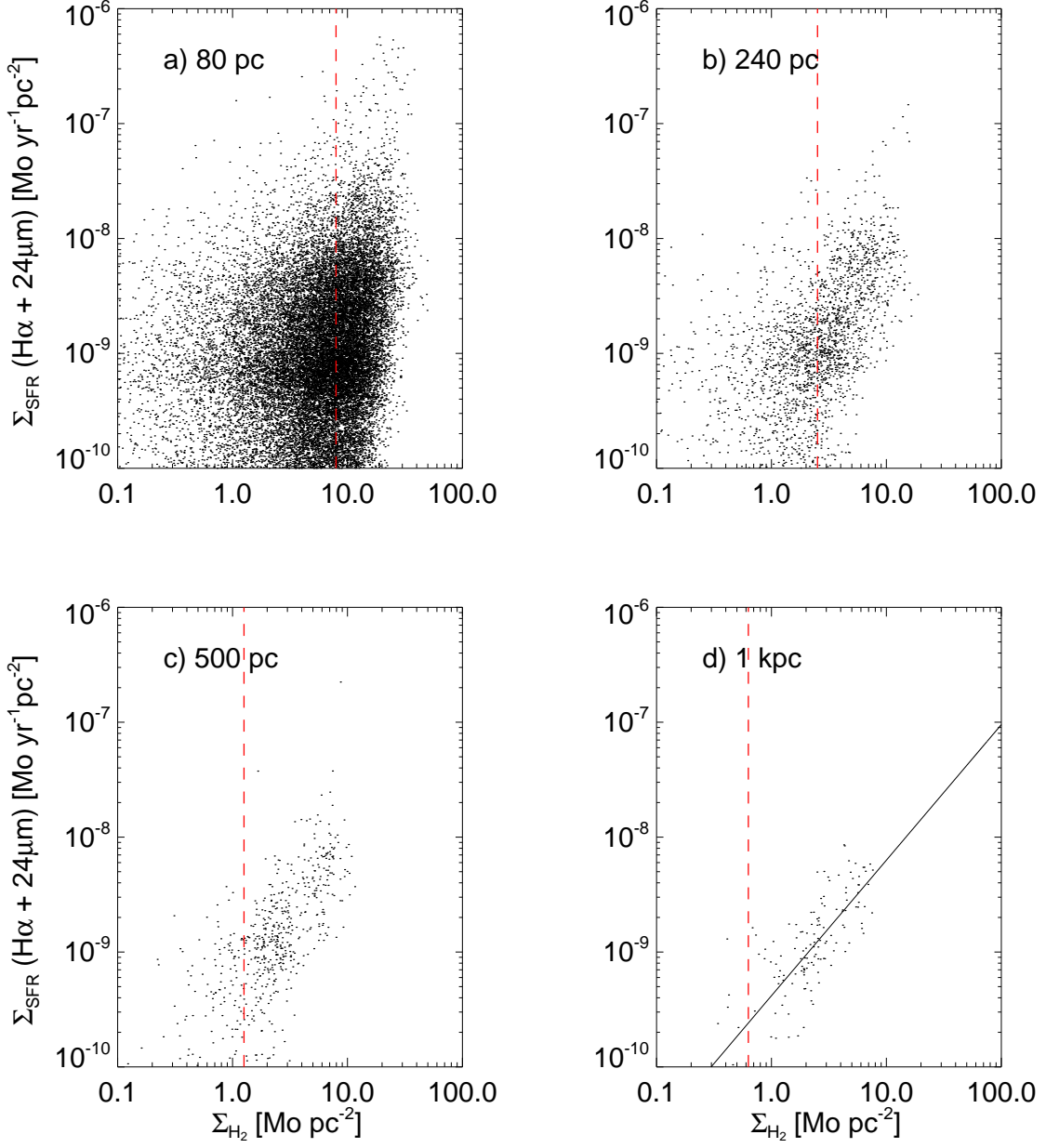


FIG. 3.— Star formation rate per unit area (Σ_{SFR}) versus surface density of H_2 gas (Σ_{H_2}) for four different resolutions: (a) $19''.3$ ($\sim 80\text{pc}$), (b) $60''$ ($\sim 240\text{pc}$), (c) $120''$ ($\sim 500\text{pc}$), and (d) $240''$ ($\sim 1\text{kpc}$). The broken red lines in each panel represent $\Sigma_{\text{H}_2} = 2\sigma$ of the maps. The line in the lower-right panel represents the best least-squares fit to the $\sim 1\text{kpc}$ resolution data; $\log \Sigma_{\text{SFR}} = (1.18 \pm 0.11) \log \Sigma_{\text{H}_2} - (9.38 \pm 0.05)$. The data points with $\Sigma_{\text{H}_2} < 2\sigma$ are not used for the fitting.